

# Resonance Raman and temperature-dependent electronic absorption spectra of cavity and noncavity models of the hydrated electron

Jennifer R. Casey<sup>a</sup>, Ross E. Larsen<sup>b</sup>, and Benjamin J. Schwartz<sup>a,1</sup>

<sup>a</sup>Department of Chemistry and Biochemistry, University of California, Los Angeles, Los Angeles, CA 90095; and <sup>b</sup>Computational Science Center, National Renewable Energy Laboratory, Golden, CO 80401

Edited by Peter J. Rossky, University of Texas at Austin, Austin, TX, and approved December 26, 2012 (received for review November 7, 2012)

Most of what is known about the structure of the hydrated electron comes from mixed quantum/classical simulations, which depend on the pseudopotential that couples the quantum electron to the classical water molecules. These potentials usually are highly repulsive, producing cavity-bound hydrated electrons that break the local water H-bonding structure. However, we recently developed a more attractive potential, which produces a hydrated electron that encompasses a region of enhanced water density. Both our noncavity and the various cavity models predict similar experimental observables. In this paper, we work to distinguish between these models by studying both the temperature dependence of the optical absorption spectrum, which provides insight into the balance of the attractive and repulsive terms in the potential, and the resonance Raman spectrum, which provides a direct measure of the local H-bonding environment near the electron. We find that only our noncavity model can capture the experimental red shift of the hydrated electron's absorption spectrum with increasing temperature at constant density. Cavity models of the hydrated electron predict a solvation structure similar to that of the larger aqueous halides, leading to a Raman O–H stretching band that is blue-shifted and narrower than that of bulk water. In contrast, experiments show the hydrated electron has a broader and red-shifted O–H stretching band compared with bulk water, a feature recovered by our noncavity model. We conclude that although our noncavity model does not provide perfect quantitative agreement with experiment, the hydrated electron must have a significant degree of noncavity character.

solvated electron | quantum simulation | Raman spectroscopy | optical spectroscopy

The hydrated electron is the simplest quantum mechanical solute, consisting of an excess electron in liquid water. Because of its apparent simplicity, the hydrated electron provides a unique opportunity for confrontation between experiments and quantum simulations. However, despite nearly five decades of interest in the hydrated electron, there is still controversy over the nature of its molecular structure (1–14). Experimental observables, such as the absorption spectrum of the hydrated electron at different temperatures and pressures (12, 13) or the results of ultrafast pump-probe experiments on the hydrated electron, provide only indirect clues to the electron's molecular structure. One of the few experiments that offered a definite possible structure was electron spin-echo envelope modulation measurements on excess electrons in aqueous alkaline glassy matrices at 77 K (1). These experiments suggested that the electron is localized in a cavity that contains no water molecules, and that there are six surrounding water molecules in an octahedral geometry around the cavity, each with an O–H bond oriented toward the electron; this arrangement has been referred to as the “Kevan structure.” It is not clear, however, how transferrable results from frozen aqueous alkaline glasses are to hydrated electrons in room-temperature liquid water, and there is surprisingly little structural information that can be inferred directly from most other experiments.

Thus, most of the evidence for assigning particular structures to the hydrated electron has come from quantum molecular dynamics (MD) simulations. One of the earliest mixed-quantum/classical (MQC) simulations of the hydrated electron was performed by Schnitker and Rossky (SR), who used a pseudopotential whose derivation was later shown to contain an error, albeit one that did not qualitatively change the nature of their results (15). With their potential, SR found that the hydrated electron, on average, had the Kevan structure, with the electron in a cavity and roughly octahedrally coordinated by six bond-oriented water molecules (3, 16). A few years later, Turi, Borgis, and their coworkers (TB) developed a more rigorous electron–water interaction potential and also found a simulated hydrated electron that occupied a cavity in the solvent, but the water structure around the cavity was somewhat less defined than seen with the SR model, and the first solvent shell contained only roughly four water molecules instead of six (9). Jacobson and Herbert (17) recently extended the TB model to incorporate electronically polarizable water but found little difference in structure from that seen by TB. Fully ab initio simulations of the hydrated electron largely have been limited to just a few explicitly treated water molecules and have been based on density functional theory (DFT) functionals that may not be appropriate for treating an unbound electron (18); these simulations also have suggested that the electron occupies a cavity, albeit highly fluxional and distorted. There also has been a large variety of both experimental and theoretical work studying the structure of gas-phase water anion clusters, but the way the behavior of such clusters extrapolates to that of the hydrated electron in bulk water with cluster size has been highly controversial (19).

Although almost all the theoretical work to date suggests that the hydrated electron occupies a cavity, we recently challenged this idea by suggesting a picture in which the hydrated electron is associated with a region of enhanced water density (14). Even though there are roughly 30 water molecules occupying the space inside most of the hydrated electron's wave function, this picture also appears consistent with experiment. We found this unusual noncavity behavior when developing a pseudopotential that includes repulsive terms between the water H atoms and attractive terms behind the water O atom that were not included in previous potentials but are necessary to guarantee orthogonality between the excess electron's wave function and the electrons in the occupied water molecular orbitals; our potential has since been referred to as the “LGS model.” Our proposal that a noncavity model should be considered on par with the various cavity models, however, has met with some resistance (20–22). Part of the objections to our proposed possible noncavity picture stem from technical

Author contributions: B.J.S. designed research; J.R.C. and R.E.L. performed research; J.R.C. and R.E.L. analyzed data; and J.R.C. and B.J.S. wrote the paper.

The authors declare no conflict of interest.

This article is a PNAS Direct Submission.

<sup>1</sup>To whom correspondence should be addressed. E-mail: schwartz@chem.ucla.edu.

This article contains supporting information online at [www.pnas.org/lookup/suppl/doi:10.1073/pnas.1219438110/-DCSupplemental](http://www.pnas.org/lookup/suppl/doi:10.1073/pnas.1219438110/-DCSupplemental).

issues, such as whether the electron–water pseudopotential should be analytically fitted to better represent the physical features found in the true potential or to better reproduce the eigenenergy for a single water anion (23). In addition, Turi and Madarász (20) found that small changes in the balance of attractive and repulsive terms in the pseudopotential can change whether the resulting hydrated electron occupies a cavity; this extreme sensitivity to minute details in the potential suggests that caution is warranted when inferring any structural model from the details of a mixed quantum/classical simulation (23).

It is worth noting that our group certainly was not the first to suggest that the hydrated electron may not reside in a cavity (5), and the idea that there may be water molecules interior to the wave function of the hydrated electron also was extended recently by Jungwirth and coworkers (24). These workers performed DFT-based ab initio MD simulations of the hydrated electron with 64 waters treated quantum mechanically and hundreds more treated classically, and found that the resulting hydrated electron had both cavity and noncavity features: the central cavity was significantly smaller than that predicted by either the SR or TB model, and well over half the electron density resided outside the central cavity and overlapped the surrounding water (24). Thus, even ab initio work suggests that it is not unreasonable for the hydrated electron to have interior water molecules, leaving open the question as to whether a cavity, noncavity, or possibly a hybrid picture is the best for describing the molecular structure of the hydrated electron.

In this paper, we work to better understand the structure of the hydrated electron by making some more rigorous comparisons between experiment and the simulated cavity and noncavity pictures of the hydrated electron. First, we examine the temperature and density dependence of the hydrated electron's absorption spectrum, because this provides an exquisite measure of the balance between the attractive and repulsive terms in the underlying potential. What we find is that the SR and TB cavity models of the hydrated electron cannot reproduce the experimental linear red shift of the hydrated electron's absorption spectrum with increasing temperature at constant density. In contrast, our noncavity LGS model does show a linear red shift, but the slope is roughly twice as large as experiment. This suggests that cavity models underestimate the attractive terms in the potential, whereas our noncavity model overestimates these terms. Second, we focus on connections between simulations and the experimental resonance Raman spectrum of the hydrated electron. We find that the TB and SR cavity models of the hydrated electron predict O–H stretching bands for the nearby water molecules that are narrower than that of bulk water, with most of the enhanced intensity on the blue side of the bulk water band, a result that is in poor qualitative agreement with experiment. In contrast, our noncavity LGS potential predicts an O–H stretching band that is broader than that of bulk water and enhanced on the low-frequency side, in excellent qualitative agreement with experiment. Together, the results indicate that the correct picture of the hydrated electron must include significant overlap between the hydrated electron and the solvating water molecules to obtain qualitative agreement with experiment.

## Results

To compare various simulation models of the hydrated electron to experiment, we performed MQC MD simulations of one quantum mechanical electron and 499 classical flexible simple point charge (SPC) (25) water molecules. As in all the previous work done in this area (2, 4, 9, 10, 14), we chose to perform our MQC simulations in the microcanonical ensemble, which provided an average temperature with  $\sim 5$  K fluctuations (see [Supporting Information](#) for details). The system was confined to a cubic box of length 24.64 Å with periodic boundary conditions, and all interactions were tapered using a spherical cutoff centered at the oxygen atom. The quantum mechanical wave function of the excess electron was expressed on a cubic grid of length 18.17 Å; we found that  $16^3$  grid points were satisfactory to describe the

electron with the SR and TB potentials but that our noncavity LGS potential required  $32^3$  grid points. The adiabatic eigenstates were found at every time step using the Lanczos algorithm, and the quantum forces were evaluated using the Hellmann-Feynman theorem with the Verlet algorithm used to propagate dynamics with a 0.5-fs time step. Additional computational details, including the way we construct the optical absorption and resonance Raman spectra of the various hydrated electron models, are presented in [Supporting Information](#).

Before discussing how the fundamental differences in the SR, TB, and LGS models lead to differences in predicted experimental observables, we begin by quickly reviewing the structural properties of the three models. In all three models, the electron has a roughly spherical wave function with a radius of gyration of  $\sim 2.2$ – $2.4$  Å, in reasonable agreement with experimental estimates based on spectral moment analysis (12). This explains why all three models do a satisfactory job of reproducing the experimental absorption spectrum. Despite the similarities in charge density, however, the three models predict very different molecular structures for the hydrated electron. In Fig. 1, we plot radial distribution functions to gauge the positions of both the water O atom (black solid curves) and H atom (red dotted curves) sites relative to the hydrated electron's center of mass (COM) for each of the three models. The SR and TB models (Fig. 1A) both show a cavity-bound electron with the SR cavity being marginally larger than the TB cavity. The SR and TB radial distribution functions resemble those of the larger halides in water (26, 27), except that the structure around the electron is somewhat less well defined. In contrast, the radial distribution functions for the LGS electron (Fig. 1B) show water molecules residing well inside the electron density as a result of the inclusion of attractive forces that were neglected in the SR and TB models (14). With the “first-shell” water molecules experiencing such fundamentally different environments for the cavity and noncavity models, it seems it would be simple to determine which picture is more accurate via experiment, but thus far comparison with experiment supports both models about equally well (14). Fortunately, the differences in attraction between the electron and the local water environment can be probed by the temperature dependence of the electronic absorption spectrum, and the resonance Raman spectrum provides a measure of the local water H-bonding structure around the hydrated electron.

**Temperature-Dependent Absorption Spectra of Different Models of the Hydrated Electron.** Because many of the questions concerning the different models of the hydrated electron revolve around the balance of attractive and repulsive terms in the electron–water pseudopotential (20), we begin our discussion by focusing on calculating the properties of different models of the hydrated electron as a function of temperature. This is because at constant density, solutes that have predominantly repulsive interactions with solvent

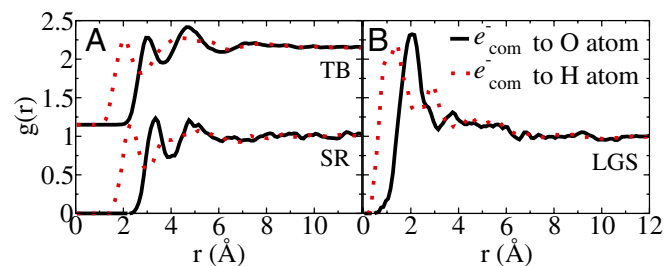


**Fig. 1.** The radial distribution function of the electron COM to both O atom (black solid curves) and H atom sites (red dotted curves) for the (A) SR and TB (offset by 1.15 for clarity) and (B) LGS models of the hydrated electron at  $\sim 298$  K and a density of 0.997 g/mL. The SR and TB models show a distinct cavity, whereas the LGS model shows water molecules residing near the electron COM.

molecules will have properties that are highly insensitive to temperature, whereas solutes that have predominantly attractive interactions with solvent molecules will have highly temperature-dependent properties (28). After all, systems that are dominated entirely by repulsive forces (e.g., the hard sphere fluid) do not even have a well-defined temperature, but their structure is highly sensitive to the density. In contrast, temperature starts to make a difference in structure at fixed density when repulsive interactions are softened and/or attractive interactions are introduced. Thus, the temperature dependence of the hydrated electron's absorption spectrum at constant density should provide an excellent metric of the correct balance between the attractive and repulsive terms in any given model for electron–water interactions.

The absorption spectrum of the hydrated electron at room temperature and density consists of a broad, featureless band that spans the visible and near-IR wavelength ranges with an absorption maximum ( $E_{\max}$ ) of 1.72 eV. The spectrum is known to fit empirically to a Gaussian function on the low-energy side of  $E_{\max}$  and a Lorentzian function on the high-energy side (29). Both the TB and LGS potentials predict absorption spectra for the hydrated electron that are in generally good agreement with experiment, although the TB model predicts a spectrum that is slightly blue-shifted from experiment (9) whereas the LGS-predicted spectrum is slightly red-shifted (14). The original SR potential produces an optical absorption band for the hydrated electron that is quite blue-shifted (by  $\sim 0.7$  eV) relative to experiment (16), although the SR model's absorption spectrum shifts into better agreement with experiment when the mathematical error in its derivation is corrected (15). Of greater interest for the present purpose is the fact that the hydrated electron's optical absorption band undergoes a roughly linear red shift with increasing temperature; this red shift happens both at atmospheric pressure (13) and at pressures into the supercritical regime (12), with a noticeable change in  $E_{\max}$  of the electron's spectrum even for relatively small (a few kelvins) changes in  $T$ .

Several groups have attempted to understand this temperature dependence of the hydrated electron's absorption spectrum on the basis of MQC simulation models. Berne and coworkers (4) developed a repulsive electron–water interaction potential that produced a cavity hydrated electron, and found that although the calculated absorption spectrum of the electron with this potential was in reasonable agreement with experiment at room temperature, this model produced no shift in the electron's spectrum, even after the temperature was increased 73 K. Golden and Tuttle (5) commented on the inability of early cavity models to capture the essence of the experimental optical absorption spectrum of the hydrated electron and suggested that a solvent–anion complex might prove to be more consistent with experiment. Subsequently, Borgis and coworkers (10) performed temperature-dependent simulations of the hydrated electron using the cavity-forming TB model, and found that the electron's spectrum shifted slightly to the blue with increasing temperature at constant density, the opposite of what is seen experimentally. These authors noted, however, that real water undergoes a density change when the temperature is varied at constant pressure, and that some of the observed red shift of the electron's spectrum could be recovered when the constant-volume simulations were constructed to allow the water density to vary in a manner similar to experiment. Thus, Borgis and coworkers (10) concluded that the observed red shift of the electron's spectrum with temperature is not actually a temperature effect but instead is a density effect.

Although this conclusion appeared to make sense, subsequent experiments showed that the observed red shift of the electron's spectrum indeed is truly a temperature effect. First, Bartels et al. (12) examined the spectrum of the hydrated electron in supercritical water at constant temperature and found only a small change in  $E_{\max}$  over a 0.5-g/mL change in density. Second, another experiment from this same group took advantage of the facts that water has a density maximum at 4 °C and that water can be supercooled easily; this allowed these authors to examine the

spectrum of the hydrated electron at pairs of points on opposite sides of the density maximum that have the same density but different temperatures. These workers found that the absorption spectrum of the hydrated electron red-shifted by 0.12 eV between  $-18$  °C and 32.6 °C, state points at atmospheric pressure where water has a density of 0.9947 g/mL (13). Additional experiments led Bartels and coworkers (13) to conclude that the absorption maximum of the hydrated electron's spectrum shifts by 0.0022 eV/K, independent of the water density; this comprises a fairly substantial constant-density temperature dependence.

To better understand how different simulation models reproduce the experimental temperature dependence of the hydrated electron's absorption spectrum, we ran MQC simulations of the SR, TB, and LGS models of the hydrated electron in the microcanonical ensemble at temperatures of  $\sim 300$  K, 325 K, 350 K, and 370 K at a constant density of 0.997 g/mL, and also at the experimental densities for each temperature for water at 1 atm pressure (*Supporting Information*). The calculated absorption spectra of the hydrated electron from the constant-density simulations are shown in Fig. 2; the changes in  $E_{\max}$  with temperature found from fitting the calculated spectra to the standard Gauss-Lorentzian form are summarized in Fig. 3, with least-squares-fitted lines drawn through the data points. For these constant-density simulations, both the cavity-forming SR (Fig. 3, green line, shifted into better agreement with experiment by 0.5 eV) and TB (Fig. 3, blue line, shifted into better agreement with experiment by 0.25 eV) potentials predict that the maximum of the hydrated electron's absorption spectrum effectively does not change with increasing temperature, in contrast to experiment (Fig. 3, black curve, see ref. 13), which shows a clear red shift with increasing temperature at constant density. Our noncavity LGS model (Fig. 3, purple line, data not shifted), in contrast, can correctly predict a substantial red shift in the optical absorption spectrum of the hydrated electron with increasing temperature at constant density. Moreover, the shift of  $E_{\max}$  with  $T$  for the LGS model is indeed quite linear, also in good agreement with experiment, but the slope of the shift for the LGS-calculated spectrum is 0.0052 eV/K, about a factor of 2.4 larger than what is observed experimentally.

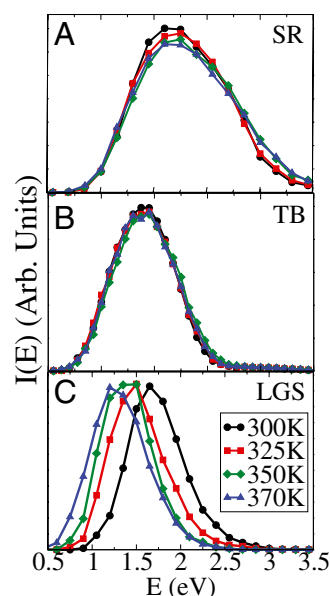


**Fig. 2.** Calculated absorption spectra for the (A) SR, (B) TB, and (C) LGS models of the hydrated electron at  $\sim 300$  K (black  $\bullet$ ),  $\sim 325$  K (red  $\blacksquare$ ),  $\sim 350$  K (green  $\blacklozenge$ ), and  $\sim 370$  K (blue  $\blacktriangle$ ) at a constant density of 0.997 g/mL. Only the LGS noncavity model captures the experimentally observed red shift with increasing temperature at constant density; see also Fig. 3.

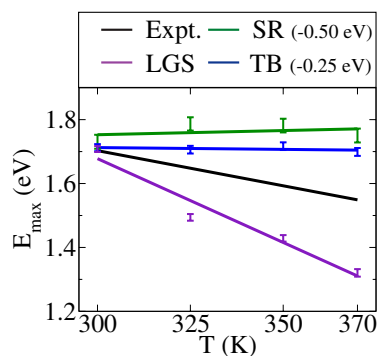


**Fig. 3.** The peak of the hydrated electron's absorption spectrum,  $E_{\max}$ , plotted against  $T$  for water held at a fixed density of 0.997 g/mL. The black line shows the experimentally measured results (13). For the different simulation models,  $E_{\max}$  and the error bars (representing the 95% confidence interval) were determined by fitting the data in Fig. 2 to the standard Gauss-Lorentz form, yielding values for the SR model (green points,  $E_{\max}$  shifted by 0.5 eV into better agreement with experiment), TB model (blue points,  $E_{\max}$  shifted by 0.25 eV into better agreement with experiment), and LGS model (purple points, data not shifted); the colored lines drawn through the points are linear least-squares fits to the data.

Taken together, the data in Fig. 3 allow us to conclude that cavity-forming hydrated electron models, such as those of Berne and coworkers (4), SR, and TB, contain electron-water interactions that are too repulsive: none of these three models shows a significant  $T$  dependence for the hydrated electron's spectrum at constant density, a result in direct contrast to experiment. This means all these models significantly underestimate the role of attractive interactions in the electron-water interaction, and it is these attractive interactions that are responsible for the non-cavity behavior seen with the LGS model (20, 23). The LGS potential appears to provide a qualitatively correct prediction of the behavior of the experimental hydrated electron, but the fact that the  $T$  dependence is overestimated suggests that the LGS potential somewhat overemphasizes the attractive terms in the electron-water interaction. This observation is consistent with the fact that the LGS potential slightly overbinds the electron both to a single water molecule (20) and to small water anion clusters (21). Thus, our conclusion from this section is that none of the water-electron pseudopotentials produced to date have done a proper job of balancing the attractive and repulsive interactions (23) but that the LGS potential is the only one tested for temperature and density dependence thus far that includes attractive terms that are sufficient to provide a meaningful connection to experiment.

#### Modeling the Resonance Raman Spectrum of the Hydrated Electron.

Resonance Raman spectroscopy is one of the few experiments that directly addresses the structure of the hydrated electron in room-temperature liquid water. The experiments by Tauber and Mathies (6, 8) and Tahara and coworkers (30) found that the water vibrations that were resonantly enhanced upon excitation of the hydrated electron were virtually identical to those of bulk liquid water, indicating that the hydrated electron's wave function resides predominantly between water molecules and does not significantly perturb the water's electronic structure. The resonance Raman spectrum of water associated with the hydrated electron does show a slight red shift of the bending vibration and a broadening and enhancement on the red side of the O-H stretching vibration; the experimental data from ref. 11 are reproduced as the circles/black curve in Fig. 4. In addition, resonance Raman studies of hydrated electrons in isotopically labeled water have shown a splitting of the water bending vibration. This indicates that the H atoms on any given molecule surrounding the hydrated electron experience different local environments, so there must be some net H-bond orientation

toward the electron (11). For liquid water, it is well established that water molecules that make strong hydrogen bonds have lower O-H stretching frequencies, whereas water molecules that make weaker H-bonds have higher O-H stretching frequencies. The fact that the O-H stretches of the water molecules closest to the hydrated electron are broadened compared with those of bulk water thus suggests that these molecules experience a wider variety of H-bonding environments than when no electron is present, and the enhancement seen at lower frequencies indicates that most of the water molecules nearest the electron experience H-bonds that are stronger than those experienced by water molecules in the bulk.

Given that the resonance Raman spectrum contains information about the local water H-bonding and thus the structure of the hydrated electron, we extended the semiclassical method developed by Skinner and coworkers (31–33) to calculate the resonance Raman spectrum of the SR, TB, and LGS models of the hydrated electron; the details of how we calculated the resonance Raman spectra are given in *Supporting Information*. Fig. 4 shows that the SR (green squares/curve) cavity model of the hydrated electron predicts a resonance Raman spectrum for the O-H stretch that is both narrower and preferentially enhanced on the blue side relative to the spectrum in bulk flexible SPC water (red plus signs/curve). This predicted narrowing of the spectrum, which is in contrast to experiment, is perhaps not surprising. Our calculations show that for the SR model, which predicts the Kevan structure for the hydrated electron, the closest six waters contribute most significantly to the resonance Raman spectrum (*Supporting Information*), and these six waters are all in roughly equivalent environments given the near-octahedral symmetry of the structure predicted by this model. This homogeneity of the first-shell water environments explains why the predicted resonance Raman spectrum for the SR electron is narrower than for the bulk. That the six closest water molecules in the SR model have a blue-shifted Raman spectrum is a consequence of the fact that these water molecules interact more weakly with the hydrated electron than they would with another H-bonding water molecule. This is because for SPC water, the O atom from a water molecule that makes an H-bond to another water molecule carries a charge of  $-0.8e$  at a distance of  $\sim 1.6$  Å, whereas if one uses Gauss' law and assumes that a cavity hydrated electron can be treated as a point charge at its

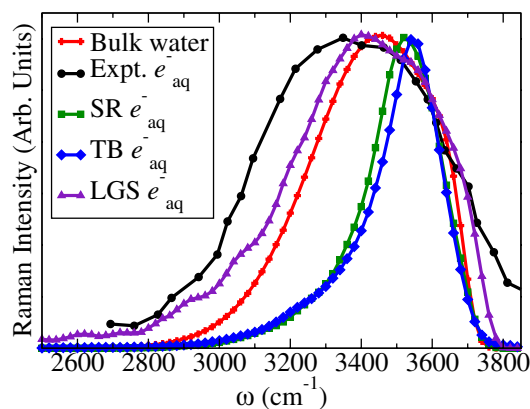


**Fig. 4.** The experimental resonance Raman spectrum of the hydrated electron (black ●/curve, from ref. 11) compared with the calculated Raman spectrum of bulk SPC/Flex water (red +/curve) and the force-weighted calculated resonance Raman spectra of the SR (green ■/curve), TB (blue ◆/curve), and LGS (purple ▲/curve) models of the hydrated electron. Both the SR and TB models produce Raman spectra that are blue-shifted and narrowed compared with the bulk, in stark contrast to the experiment, whereas the LGS model correctly predicts that the Raman spectrum of the hydrated electron should be both broader and red-shifted relative to that of bulk water.

center of mass, then the electron carries a charge of  $-1 e$  at a distance of  $\sim 2.1 \text{ \AA}$  from the nearest H atoms. Because the electric field goes inversely with the square of the distance (Eq. S4), this simple argument explains why the cavity electron is a poorer H-bond than water, and thus why the SR model predicts a narrowed, blue-shifted O–H stretching spectrum that is in contrast to experiment.

A similar argument may be used to explain the poor agreement between the predicted O–H Raman stretch for the TB model (Fig. 4, blue diamonds/curve) and experiment. Like the SR model, the roughly four first-shell water molecules in the TB model make poorer H-bonds to the electron in the cavity compared with the H-bonds they would make with other water molecules. These molecules are the ones that experience the largest force difference upon excitation of the electron (Supporting Information), so they are the molecules that dominate the observed resonance-enhanced O–H stretch, explaining the blue-shifted and narrowed predicted spectrum. We note that the water molecules in the TB electron are slightly closer to the electron's COM than those in the SR model, but more of the electron's wave function lies outside the first-shell H atoms in the TB model relative to the SR model, so the electron makes roughly equally poor H-bonds to the four first-shell water molecules around the TB cavity as to the six water molecules around the SR cavity. In essence, cavity models of the hydrated electron intrinsically assume that the electron significantly breaks the local structure of water's H-bonding network, and this disruption of the network is not consistent with the broadening and enhancement of lower-frequency O–H stretches seen experimentally.

In retrospect, the blue shift and narrowing of the resonance Raman spectra predicted by the SR and TB cavity models is not all that surprising. A cavity electron is similar in shape and intermediate in size to halide ions such as  $\text{Cl}^-$  and  $\text{Br}^-$ ; indeed, as mentioned above, the radial distribution functions of the water molecules around the SR and TB electrons are quite similar to those of the larger halides (2). It is well known that the presence of halides in water alters the Raman spectrum of the water's O–H stretch, with O–H Raman spectra of the larger aqueous halides that are blue-shifted and narrowed compared with that of bulk water (26, 27). This effect has been ascribed to the fact that halide ions break the local H-bonding structure of the surrounding water molecules: the water molecules in the halide's first solvation shell orient an O–H bond toward the anion, so that both the first- and second-shell water molecules make weaker H-bonds (both to the halide ion and to the neighboring water molecules), thus raising the average frequency of the O–H stretch in a manner that increases with the size of the halide ion (26). Because a cavity hydrated electron is intermediate in size to  $\text{Cl}^-$  and  $\text{Br}^-$  and breaks the local water structure in a similar way, it is thus not surprising that it should have a Raman spectrum of the O–H stretch that is similar to that of the larger halides. Interestingly, however, aqueous  $\text{F}^-$  (and also aqueous hydroxide) has an O–H Raman spectrum that is red-shifted and broadened relative to that of bulk water (26, 27, 34), very similar to that observed for the hydrated electron. The Raman spectra of  $\text{F}^-$  and  $\text{OH}^-$  have been explained as resulting from significant electron transfer from the anion to the surrounding water molecules, so the anionic charge distribution encompasses the first-shell waters. Thus, based on the Raman spectrum of the water O–H stretch, one might expect the hydrated electron to have a structure that resembles  $\text{F}^-$  or  $\text{OH}^-$  rather than the larger halides, with little breaking of the local H-bonding and a delocalized charge distribution (35), both of which are represented better by a noncavity model than by a cavity model for the hydrated electron.

Thus, in contrast to the cavity models, our LGS potential can capture both the broadening and the enhancement on the lower-frequency side of the hydrated electron's O–H stretch resonance Raman spectrum, as seen in Fig. 4 (purple triangles/curve). The predicted O–H stretching band for the LGS model may be rationalized by the fact that most of the water molecules inside the

hydrated electron's wave function contribute to the resonance Raman spectrum (Supporting Information). Because these water molecules in the LGS electron are compressed by electrostriction to a higher density than the bulk (14), they have stronger H-bonds, on average, than water in the bulk, explaining the low-frequency enhancement of their O–H stretches. In addition, the water molecules inside the noncavity LGS hydrated electron maintain their H-bonding network (14), explaining why, unlike the structure-breaking cavity models, the full width of the O–H stretching band is preserved in the predicted LGS resonance Raman spectrum. Moreover, the fact that the LGS hydrated electron's wave function decays from the center outward means that the water molecules inside the electron experience a significant electric field gradient. Most of these interior waters are oriented with H-bonds pointing toward the electron's COM (14), so for these waters, the electric field gradient from the electron enhances their O–H bonding and thus further lowers the O–H stretching frequency, providing an additional reason why the predicted spectrum is enhanced on the low-frequency side. However, unlike the cavity models, some of the waters in the interior of the LGS electron have O–H bonds oriented against the electric field gradient, so these waters experience effectively weaker H-bonds and thus show blue-shifted O–H stretching frequencies, explaining why the predicted O–H stretching band for the LGS electron is slightly broader than that in bulk water.

In summary, the data in Fig. 4 show that the cavity models of the hydrated electron tested here do not predict resonance Raman spectra for the O–H stretch that are consistent with experiment: the experimentally observed red shift of the O–H stretch simply is inconsistent with the disrupted H-bond network that would accompany confinement of the hydrated electron in a cavity. Moreover, the homogeneous environment of the first-shell waters that make H-bonds to the electron in cavity models would predict a narrowing of the Raman O–H stretching spectrum, a result that again is in contrast to experiment. Our noncavity LGS electron, on the other hand, predicts a resonance Raman spectrum for the O–H stretch that is in excellent qualitative agreement with experiment, explaining both the broadening of the band and the preferential enhancement of intensity on the low-frequency side. We note that  $(\text{H}_2\text{O})_2^-$  also shows a similar broadening and red shift of the O–H stretch (36), suggesting that overlap between the electron and water wave functions also might be responsible for the redshift, an idea we plan to investigate in the future. Thus, even though the predicted resonance Raman spectrum for our LGS model is not in quantitative agreement with experiment, the results presented above suggest that a noncavity model is in much better line with the experimentally observed vibrational structure of the hydrated electron than a cavity model.

## Conclusions

From the studies we have done on both the temperature dependence of the absorption spectrum and the resonance Raman spectrum of the hydrated electron, it seems clear that our noncavity picture is superior in making contact with experiment relative to the cavity models tested here. In the SR and TB cavity models, the electron resides in a repulsive and rigid cavity, leading to a lack of temperature dependence of the absorption spectrum and a narrowed and blue-shifted O–H stretch in the resonance Raman spectrum, both of which are in contrast to experiment. Our LGS potential is found to be somewhat too attractive, as was pointed out previously (20, 21, 23), in that it overestimates the temperature dependence of the hydrated electron's absorption spectrum, but at least it shows a temperature dependence with the correct sign and order of magnitude; thus, we consider the general agreement to be satisfactory. Perhaps more importantly, the fact that a noncavity model such as LGS can predict a resonance Raman spectrum that is consistent with experiment whereas cavity-forming models cannot is to us a clear sign that the structure of the hydrated electron must have significant noncavity character.

As mentioned in the introduction, recent ab initio MD simulations by Jungwirth and coworkers (24) have suggested a structure that is something of a compromise between the cavity and noncavity pictures of the hydrated electron. The computational expense of this type of model makes calculating the temperature dependence of the absorption spectrum computationally prohibitive. However, for this hybrid structural picture, the facts that the electron density overlaps with the closest water molecules (as with our LGS model) and that the structure of the surrounding water is less broken than the cavity models suggest that such a hybrid structure might be more consistent with the experimental resonance Raman spectrum than the cavity models. On the other hand, the fact that only a fraction of the electron's charge density overlaps with the nearby waters also suggests that there may not be enough of an electric field gradient to produce the broadening of the spectrum seen both experimentally and with the LGS model. Calculations of the Raman spectrum for this hybrid model of the hydrated electron are under way.

Finally, we note that as long as we are restricted to a one-electron picture to do extensive calculations to compare with experiment, the structure of the hydrated electron we predict from such models will be determined by subtleties in the pseudopotential that may be difficult to capture. Clearly, potentials that are too repulsive lead to cavity hydrated electrons whose Raman spectra do not agree well with experiment, whereas potentials that are too attractive lead to an overbound electron for which the temperature dependence of the absorption spectrum is overstated relative to experiment. The "true" one-electron potential, if any such thing exists, clearly is somewhere in the

middle, right at the tipping point between cavity and noncavity behavior (20, 23). We believe that a problem with all one-electron models lies in the fact that they generally are derived for the interaction between an electron and an isolated gas-phase water molecule. Yes, corrections for polarizability and other condensed-phase effects can be grafted on afterward (22), but this still does not change the intrinsic problem that the electron's wave function is being forced by such potentials to be orthogonal to those of a gas-phase water molecule's molecular orbitals (MOs), even though the MOs of water molecules in liquid water are quite different from those in the gas phase (as evidenced by the change in dipole moment and vibrational frequencies of a gas-phase water molecule upon entering the condensed phase). Moreover, the MOs of a water molecule in liquid water also depend on the molecule's local environment, which means that any pseudopotential describing the electron-water interaction should be different for every water molecule. We recently developed a pseudopotential formalism that allows the potential to vary as the local environment changes, and we hope to understand how this removal of the so-called frozen core approximation affects the predicted properties of the hydrated electron in future work.

**ACKNOWLEDGMENTS.** The authors thank Argyris Kahros for helpful discussions. This work was supported by the National Science Foundation under Grant CHE-0908548. Support for the National Renewable Energy Laboratory (NREL) was provided by the US Department of Energy under Contract DE-AC36-08-GO28308 with NREL.

1. Kevan L (1981) Solvated electron structure in glassy matrices. *Acc Chem Res* 14(5):138–145.
2. Schnitker J, Rossky PJ (1987) Quantum simulation study of the hydrated electron. *J Chem Phys* 86(6):3471–3485.
3. Schnitker J, Rossky PJ (1987) An electron-water pseudopotential for condensed phase simulation. *J Chem Phys* 86(6):3462–3469.
4. Wallqvist A, Martyna G, Berne BJ (1988) Behavior of the hydrated electron at different temperatures: Structure and absorption spectrum. *J Phys Chem* 92(7):1721–1730.
5. Tuttle TR, Golden S (1991) Solvated electrons: What is solvated? *J Phys Chem* 95(15):5725–5736.
6. Tauber MJ, Mathies RA (2001) Fluorescence and resonance Raman spectra of the aqueous solvated electron. *J Phys Chem A* 105(49):10952–10960.
7. Turi L, Gaigeot MP, Levy N, Borgis D (2001) Analytical investigations of an electron-water pseudopotential. 1. Exact calculation on a model system. *J Chem Phys* 114(18):7805–7815.
8. Tauber MJ, Mathies RA (2002) Resonance Raman spectra and vibronic analysis of the aqueous solvated electron. *Chem Phys Lett* 354(5–6):518–526.
9. Turi L, Borgis D (2002) Analytical investigations of an electron-water molecule pseudopotential. 2. Development of a new pair potential and molecular dynamics simulations. *J Chem Phys* 117(13):6186–6195.
10. Nicolas C, Boutin A, Levy B, Borgis D (2003) Molecular simulation of a hydrated electron at different thermodynamic state points. *J Chem Phys* 118(21):9689–9696.
11. Tauber MJ, Mathies RA (2003) Structure of the aqueous solvated electron from resonance Raman spectroscopy: Lessons from isotopic mixtures. *J Am Chem Soc* 125(5):1394–1402.
12. Bartels DM, Takahashi K, Cline JA, Marin TW, Jonah CD (2005) Pulse radiolysis of supercritical water. 3. Spectrum and thermodynamics of the hydrated electron. *J Phys Chem A* 109(7):1299–1307.
13. Du Y, Price E, Bartels DM (2007) Solvated electron spectrum in supercooled water and ice. *Chem Phys Lett* 438(4–6):234–237.
14. Larsen RE, Glover WJ, Schwartz BJ (2010) Does the hydrated electron occupy a cavity? *Science* 329(5987):65–69.
15. Larsen RE, Glover WJ, Schwartz BJ (2009) Comment on "An electron-water pseudopotential for condensed phase simulation." *J Chem Phys* 131(3):037101.
16. Schnitker J, Rossky PJ (1988) The hydrated electron: Quantum simulation of structure, spectroscopy, and dynamics. *J Chem Phys* 92(15):4277–4285.
17. Jacobson LD, Herbert JM (2010) A one-electron model for the aqueous electron that includes many-body polarization: Bulk equilibrium structure, vertical electron binding energy, and optical absorption spectrum. *J Chem Phys* 133(15):154506.
18. Boero M, Parrinello M, Terakura K, Ikeshoji T, Liew CC (2003) First-principles molecular-dynamics simulations of a hydrated electron in normal and supercritical water. *Phys Rev Lett* 90(22):226403.
19. Neumark DM (2008) Spectroscopy and dynamics of excess electrons in clusters. *Mol Phys* 106(16–18):2183–2197.
20. Turi L, Madarász A (2011) Comment on "Does the hydrated electron occupy a cavity?" *Science* 331(6023):1387c.
21. Jacobson LD, Herbert JM (2011) Comment on "Does the hydrated electron occupy a cavity?" *Science* 331(6023):1387d.
22. Herbert JM, Jacobson LD (2011) Structure of the aqueous electron: Assessment of one-electron pseudopotential models in comparison to experimental data and time-dependent density functional theory. *J Phys Chem A* 115(50):14470–14483.
23. Larsen RE, Glover WJ, Schwartz BJ (2011) Response to comments on "Does the hydrated electron occupy a cavity?" *Science* 331(6023):1387e.
24. Uhlig F, Marsalek O, Jungwirth P (2012) Unraveling the complex nature of the hydrated electron. *J Phys Chem Lett* 3(20):3071–3075.
25. Toukan K, Rahman A (1985) Molecular-dynamics study of atomic motions in water. *Phys Rev B Condens Matter* 31(5):2643–2648.
26. Smith JD, Saykally RJ, Geissler PL (2007) The effects of dissolved halide anions on hydrogen bonding in liquid water. *J Am Chem Soc* 129(45):13847–13856.
27. Perera PN, Browder B, Ben-Amotz D (2009) Perturbations of water by alkali halide ions measured using multivariate Raman curve resolution. *J Phys Chem B* 113(7):1805–1809.
28. Andersen HC, Chandler D, Weeks JD (1976) Roles of repulsive and attractive forces in liquids: The equilibrium theory of classical fluids. *Adv Chem Phys* 34:105–156.
29. Jou FY, Freeman GR (1979) Temperature and isotope effects on the shape of the optical absorption spectrum of solvated electrons in water. *J Phys Chem* 83(18):2383–2387.
30. Mizuno M, Tahara T (2001) Novel resonance Raman enhancement of local structure around solvated electrons in water. *J Phys Chem A* 105(39):8823–8826.
31. Corcelli S-A, Lawrence C-P, Skinner J-L (2004) Combined electronic structure/molecular dynamics approach for ultrafast infrared spectroscopy of dilute HOD in liquid H<sub>2</sub>O and D<sub>2</sub>O. *J Chem Phys* 120(17):8107–8117.
32. Corcelli SA, Skinner JL (2005) Infrared and Raman line shapes of dilute HOD in liquid H<sub>2</sub>O and D<sub>2</sub>O from 10 to 90 degrees C. *J Phys Chem A* 109(28):6154–6165.
33. Auer B, Kumar R, Schmidt JR, Skinner JL (2007) Hydrogen bonding and Raman, IR, and 2D-IR spectroscopy of dilute HOD in liquid D<sub>2</sub>O. *Proc Natl Acad Sci USA* 104(36):14215–14220.
34. Robertson WH, Johnson MA (2003) Molecular aspects of halide ion hydration: The cluster approach. *Annu Rev Phys Chem* 54:173–213.
35. Thompson WH, Hynes JT (2000) Frequency shifts in the hydrogen-bonded OH stretch in halide-water clusters. The importance of charge transfer. *J Am Chem Soc* 122(26):6278–6286.
36. Wu DY, et al. (2008) Theoretical study of binding interactions and vibrational Raman spectra of water in hydrogen-bonded anionic complexes: (H<sub>2</sub>O)<sub>n</sub>- (n = 2 and 3), H<sub>2</sub>O...X- (X = F, Cl, Br, and I), and H<sub>2</sub>O...M- (M = Cu, Ag, and Au). *J Phys Chem A* 112(6):1313–1321.